ACS NANO
Cite This: ACS Nano 2018, 12, 3369−3377
www.acsnano.org

ARTICLE

Large Dielectric Constant Enhancement in MXene Percolative Polymer Composites

Shaobo Tu,[†] Qiu Jiang,[†] Xixiang Zhang,*[] and Husam N. Alshareef*[]

Materials Science and Engineering, Physical Sciences and Engineering Division, King Abdullah University of Science and Technology (KAUST), Thuwal 23955-6900, Saudi Arabia

Supporting Information

ABSTRACT: We demonstrate that poly(vinylidene fluoride) (PVDF)-based percolative composites using two-dimensional (2D) MXene nanosheets as fillers exhibit significantly enhanced dielectric permittivity. The poly(vinylidene fluoride-trifluoro-ethylene-chlorofluoroehylene) (P[VDF-TrFE-CFE]) polymer embedded with 2D $Ti_3C_2T_x$ nanosheets reaches a dielectric permittivity as high as 10^5 near the percolation limit of about 15.0 wt % MXene loading, which surpasses all previously reported composites made of carbon-based fillers in the same polymer. With up to 10 wt % MXene loading, the dielectric loss of the MXene/P(VDF-TrFE-CFE) composite indicates only an approximately 5-fold increase (from 0.06 to 0.35), while the dielectric constant increased by 25 times over the same composition range. Furthermore, the ratio of permittivity to loss factor of the MXene−polymer composite is superior to that of all previously reported fillers in this same polymer. The dielectric constant enhancement effect is demonstrated to exist in other polymers as well when loaded with MXene. We show that the dielectric constant enhancement is largely due to the charge accumulation caused by the formation of microscopic dipoles at the surfaces between the MXene sheets and the polymer matrix under an external applied electric field.

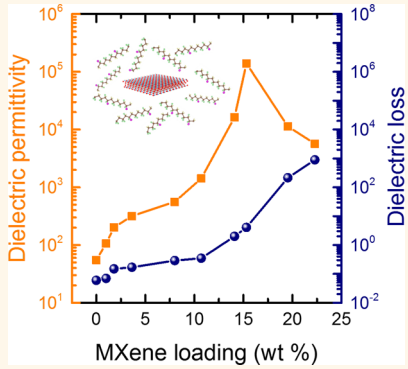

KEYWORDS: *MXene nanosheets, percolative composites, dielectric permittivities, microscopic dipoles, switching current*

Poly(vinylidene fluoride) (PVDF)-based polymers have recently attracted renewed attention for their potential in various electronic applications, including charge storage capacitors, flexible ferroelectric memories, fractional-order capacitors, nanoenergy harvesters, and strain sensors.[1−6] However, their low dielectric permittivity is one of the major factors that limits the use of these materials, especially in charge storage and fractional-order capacitor applications. Nanocomposites with insulating, semiconducting, and conducting fillers dispersed in a PVDF-based polymer matrix have been widely investigated to enhance their dielectric properties.[7] At the same time, the small volume fraction of the fillers preserves the flexibility of the polymer matrix.[8−11] In a previous report,[12] reduced graphene oxide (rGO) was used as conductive filler in a P(VDF-TrFE-CFE) matrix and resulted in a dielectric permittivity over 10 000 while maintaining a dielectric loss around 2, which was the highest dielectric constant reported for P(VDF-TrFE-CFE)-based composites.[13−16] However, to our knowledge, there have been no reports on the effect of incorporating MXene fillers in insulating polymers on their dielectric properties.

Since the discovery of MXenes in 2011,[17] researchers have heavily investigated this interesting class of two-dimensional (2D) transition metal carbides/nitrides with the general formula of $M_{n+1}X_nT_x$. In $M_{n+1}X_nT_x$, M is an early transition metal, X is carbon and/or nitrogen, T_x represents the surface functional groups (*e.g.*, OH, O, and/or F groups), and n = 1, 2, or 3. Hope *et al.* have reported that an HF-etching route results in a higher proportion of fluorine termination, which was experimentally quantified by ^{1}H and ^{19}F nuclear magnetic resonance spectroscopy.[18] The nanometer-scale dimensions and large aspect ratio make MXenes an excellent material for nanocomposite engineering. Whereas most of the reported studies have focused on enhancement of electrochemical and thermoelectric properties, no reports have been published on the dielectric properties of MXene−polymer composites.[19−23] This paper examines the effect of incorporating 2D $Ti_3C_2T_x$ nanosheets (MXene) on the dielectric performance of a PVDF-based polymer. Specifically, we demonstrate substantial enhancement of dielectric properties and propose a mechanism for enhancement based on a microscopic dipole formation model.

RESULTS AND DISCUSSION

Figure 1 illustrates the fabrication process of the MXene/P(VDF-TrFE-CFE) composite (see Methods for detailed process). Briefly, 2D $Ti_3C_2T_x$ sheets were first prepared from

Received: December 16, 2017
Accepted: April 4, 2018
Published: April 6, 2018

DOI: 10.1021/acsnano.7b08895
ACS Nano 2018, 12, 3369−3377

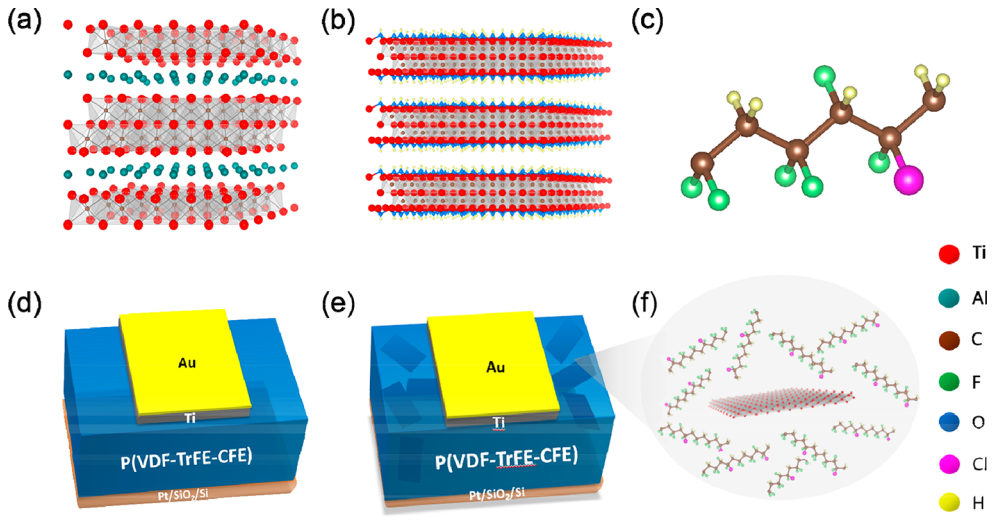

Figure 1. (a, b) Schematic illustration of the process for etching and delamination of MXene nanosheets. (c) Molecular structure of P(VDF-TrFE-CFE). (d) Schematic illustration of the capacitor device fabricated using pristine P(VDF-TrFE-CFE) as the dielectric. (e) Schematic illustration of the capacitor device fabricated using an MXene/P(VDF-TrFE-CFE) composite as the dielectric. (f) Schematic depicting the MXene sheets surrounded by polymer chains inside the composite.

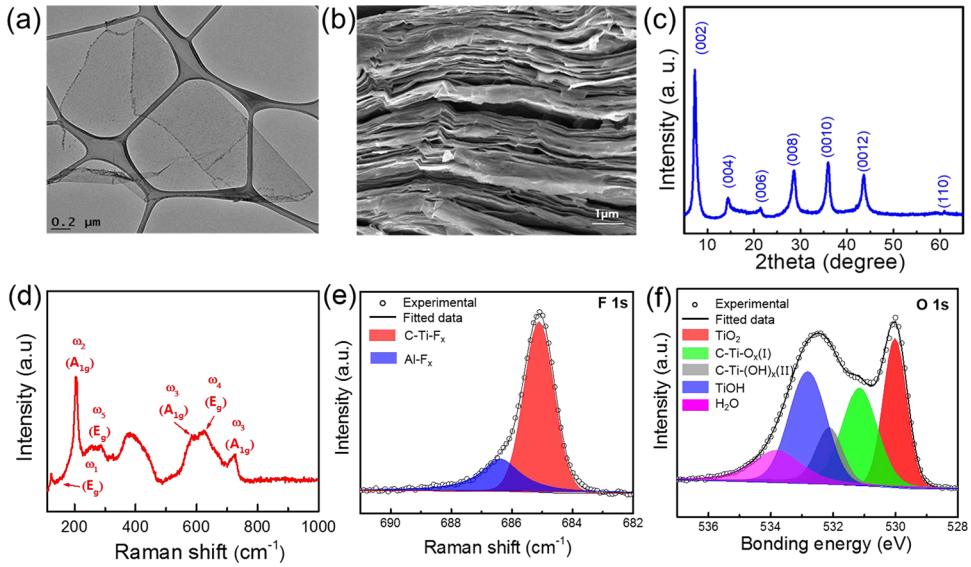

Figure 2. (a) TEM image of a single MXene sheet. (b) SEM cross-sectional image of MXene film. (c) X-ray diffraction and (d) Raman spectroscopy of $Ti_3C_2T_x$ MXene films; XPS spectra of $Ti_3C_2T_x$ MXenes (e) F 1s and (f) O 1s. Shaded colored areas signify curve-fitting results.

their bulk MAX phases using a previously reported etching and delamination method.[24] The MXene sheets were well dispersed in a polymer matrix through gentle sonication, and no aggregation was observed after leaving the solution undisturbed overnight. It is worth noting that the aggregation of MXene sheets inside the polymer matrix was observed, *via* a cross-sectional scanning electron microscopy (SEM) image, to occur at approximately 30 wt % MXene loading, and the corresponding weight percent of MXene was confirmed by thermogravimetric analysis (TGA) (see Figure S1 in the Supporting Information). A film with an average thickness of 100 μm was cast on the platinum-coated silicon substrate, as measured by a profilometer. Subsequently, Ti/Au contacts were deposited on the top of the MXene–polymer films through a shadow mask by e-beam evaporation. Figure 1e presents a schematic of a fully fabricated metal–insulator–metal (MIM) capacitor, which was used to measure the dielectric properties of MXene–polymer composites.

The transmission electron microscopy (TEM) image in Figure 2a depicts the typical morphology of a single-layer MXene sheet that has been prepared through a sequence of etching and delamination processes. Furthermore, the cross-sectional SEM image (Figure 2b) displays the layered structure of vacuum-filtrated MXene films. Raman spectroscopy and X-ray diffraction (XRD) were used to characterize the MXene sheets. $Ti_3C_2T_x$ presents a strong (002) XRD peak at $2\theta = 7.2°$ with fwhm = 0.55°, which corresponds to a *d*-spacing of 1.2 nm (see Figure 2c). As Figure 2d indicates, the Raman spectrum of $Ti_3C_2T_x$/CF exhibits strong peaks at 205 and 721 cm^{-1}, which can be assigned to the A_{1g} modes of $Ti_3C_2O_2$. The additional peaks at 128, 280, 620, and 730 cm^{-1} can be respectively assigned to the following vibrational modes: E_g of $Ti_3C_2F_2$, E_g of $Ti_3C_2(OH)_2$, E_g of $Ti_3C_2F_2$, and A_{1g} of $Ti_3C_2O_2$. These peaks

DOI: 10.1021/acsnano.7b08895
ACS Nano 2018, 12, 3369–3377

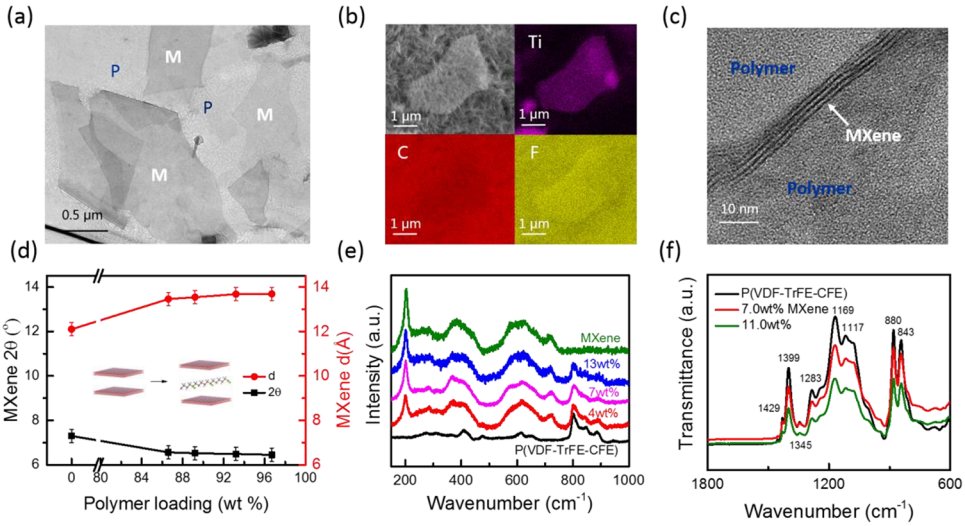

Figure 3. (a) TEM plan view image and (b) an EDS analysis of the MXene/P(VDF-TrFE-CFE) composite with 8.0 wt % MXene loading. (c) Cross-sectional TEM image depicting the edge of an MXene sheet embedded in the P(VDF-TrFE-CFE) matrix. (d) Diffraction peak angle and interlayer spacing of MXene in the P(VDF-TrFE-CFE) matrix with different polymer amounts. (e, f) Raman and FT-IR spectra of MXene/P(VDF-TrFE-CFE) composites with different MXene concentrations. M: MXene, P: polymer.

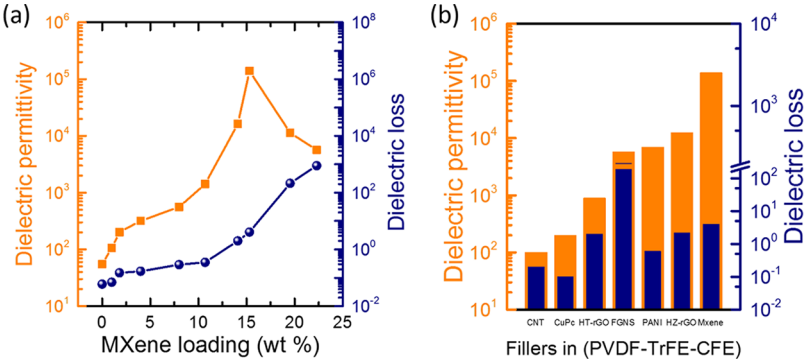

Figure 4. (a) Dependence of the permittivity and dielectric loss of the MXene/P(VDF-TrFE-CFE) on MXene content wt % measured at room temperature and 1 kHz. (b) Bar charts comparing the maximum dielectric permittivity and corresponding dielectric loss reported in the literature using P(VDF-TrFE-CFE) as a matrix with different conductive fillers.

reveal the presence of −OH, −O, and −F functional groups on the $Ti_3C_2T_x$ MXene surface.[25] Additionally, X-ray photoelectron spectroscopy (XPS) was used to characterize the surface chemistry of the samples. As Figure 2e reveals, high-resolution XPS spectra of samples in the F 1s region (685.1 eV) indicated that the $Ti_3C_2T_x$ sample contains both F-terminated Ti and AlF_x. Figure 2f illustrates that the O 1s peak can be fitted using four symmetric peaks at 530, 531, 532.2, and 532.8 eV, which respectively correspond to TiO_2, C−Ti−O_x, C−Ti−$(OH)_x$, and TiOH.[26] The peak at 533.8 eV can be attributed to H_2O.[27] See Figure S2 in the Supporting Information for the full XPS analysis.

Figure 3a presents a TEM image of MXene/P(VDF-TrFE-CFE) composite flakes that clearly indicates that the MXene sheets are randomly dispersed in the polymer matrix. In the energy dispersive spectroscopy (EDS) mapping (Figure 3b), the existence of titanium (Ti) is apparent within the MXene sheet in the center region of the P(VDF-TrFE-CFE) matrix, while C and F are prevalent over the entire region. This is because both MXene and the polymer matrix have F and C. Figure 3c displays a cross-sectional TEM image of MXene nanosheets (three layers thick) that have clearly been embedded in the polymer matrix. Figure 3d presents the XRD analysis of MXene/P(VDF-TrFE-CFE) composites with different polymer loadings. Evidently, as the polymer fraction increases, the MXene interlayer spacing expands (see also Figure S3a and Table S1 in the Supporting Information). One possible explanation for this result is the intercalation of some polymer chains between MXene layers. This intercalation may have been assisted by the functional groups on the MXene surface (*e.g.*, F, O, and/or OH), which may interact with atoms (*e.g.*, H) on the P(VDF-TrFE-CFE) chains. In fact, polymer chains can reportedly be intercalated between MXene sheets during the *in situ* polymerization process of polypyrrole (PPy).[28] Raman spectroscopy of MXene, P(VDF-TrFE-CFE), and their composites was investigated, and Figure 3e contains the corresponding data. The characteristic peaks of the composites apparently consist only of known peaks from pristine MXene and terpolymer, which suggests that there are no vibrational changes during the mixing process. As Figure 3e indicates, the intensity of the major MXene peak at 205 cm^{-1} increases at a higher MXene loading, while the intensity of the terpolymer peak at 801 cm^{-1} decreases as the MXene concentration increases. Figure 3f presents Fourier-transform infrared spectroscopy (FTIR) results for polymer composites containing different MXene loadings in transmission mode. All

DOI: 10.1021/acsnano.7b08895
ACS Nano 2018, 12, 3369−3377

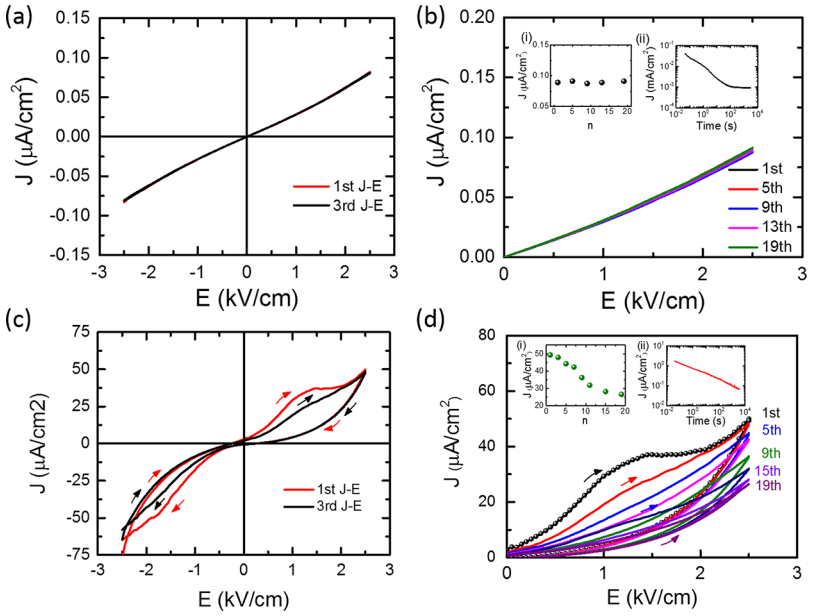

Figure 5. Pristine polymer: (a) The first *J*–*E* loop and third *J*–*E* curve of pristine P(VDF-TrFE-CFE) measured with an electric field of −2.5 to 2.5 kV cm^{-1}. (b) Unipolar *J*–*E* loops measured with a positive field on a negatively prepoled pristine P(VDF-TrFE-CFE) sample with an electric field of 2.5 kV cm^{-1}. Inset (i): Variation of the current density at maximum field with the number of cycles (*n*) of the field. Inset (ii): Time-dependent leakage current density measured under a constant field of 1.25 kV cm^{-1} for 1 h. Composite: (c) The first *J*–*E* loop and third *J*–*E* curve of the MXene/P(VDF-TrFE-CFE) (8.0 wt % MXene) composite measured with an electric field of −2.5 to 2.5 kV cm^{-1}. (d) Unipolar *J*–*E* loops measured with a positive field applied to the MXene/P(VDF-TrFE-CFE) (8.0 wt % MXene) composite, which has been prepoled with a negative field of 2.5 kV cm^{-1}. Inset (i): Decrease in the current density at maximum field with the number of cycles (*n*) of the field. Inset (ii): Time-dependent leakage current density measured under a constant field of 1.25 kV cm^{-1} for 1 h.

bands between 500 and 1500 cm^{-1} can be attributed to P(VDF-TrFE-CFE), which is consistent with previous literature reports.[29,30] No additional bands appear, while the transmittance decreases as MXene loading increases.

Figure 4a displays the dielectric permittivity and loss tangent of MXene/P(VDF-TrFE-CFE) composites as a function of filler loading. It reveals that the dielectric permittivity of both composites initially increases when the MXene filler concentration is heightened. A dielectric constant of >100 000 was reached in the case of a composite with 15.3 wt % MXene in terpolymer. A further increase in the MXene loading leads to a drop in the dielectric constant value, which indicates that we have reached the percolation limit (φ_c) for this MXene/P(VDF-TrFE-CFE) composite. According to percolation theory, for composites that contain conductive fillers embedded in an insulating polymer matrix, a power law provides the dielectric permittivity of the composite (ε_{eff}) as[31−35]

$$\varepsilon_{eff} \propto \varepsilon_m(\varphi_c - \varphi_p)^{-q} \text{ for } \varphi_p < \varphi_c \quad (1)$$

where ε_m is the dielectric constant of the insulation matrix, φ_p is the volume fraction of metallic fillers, φ_c is the volume fraction at the percolation threshold, and q is the critical exponent. The data in Figure 4a evidence that the percolation limit (φ_c) for our MXene/P(VDF-TrFE-CFE) composites occurs at 6.9 vol % (15.3 wt %) MXene loading. Table S2 notes the weight percent and volume fraction of MXene embedded in the P(VDF-TrFE-CFE) matrix.

Figure 4a additionally reveals that the dielectric loss also increases with MXene loading. An interesting observation is that the dielectric loss of the MXene/P(VDF-TrFE-CFE) composite increases approximately 5-fold (from 0.06 to 0.35) up to 10 wt % MXene loading, while the dielectric constant increases by 25 times over the same composition range. This excellent performance of the composites is best understood through a comparison of the performance of the MXene/P(VDF-TrFE-CFE) composite with published works on dielectric constant enhancement in the same polymers using a variety of fillers. Specifically, Figure 4b indicates the dielectric constant and dielectric loss of the P(VDF-TrFE-CFE) polymer in which various types of conductive fillers have been added.[36] The fillers include hydrothermally reduced graphene oxide (HT-rGO),[12] hydrazine-reduced graphene oxide (HZ-rGO),[12] carbon nanotubes (CNTs),[13] copper phthalocyanine (CuPc),[14] polyaniline (PANI),[15] and functionalized graphene nanosheets (FNGS).[16] The data of the MXene/P(VDF-TrFE-CFE) clearly stand out, as they show the best dielectric constant/loss factor trade-off among all fillers. In fact, at the same dielectric loss as HZ-rGO (∼2), the MXene-based composite shows a reasonably higher dielectric constant (15 900 *versus* 12 600). In addition, at the same loss factor of CuPc composites (0.35), MXene composites achieve a significantly higher dielectric constant (MXene 1425 *versus* CuPc 75) at 1 kHz. However, Figure 4a also illustrates that the permittivity starts to diminish when the MXene loading reaches approximately 15.3 wt %, which is near the percolation limit. The drop in the dielectric constant at higher MXene concentrations is likely due to rising leakage currents caused by increased connectivity between the MXene sheets, which leads to a transition from non-ohmic to ohmic conduction.[31] Figure S4 and Table S3 in the Supporting Information specify the dielectric constant, dielectric loss, and conductivity of MXene/P(VDF-TrFE-CFE) composites with different MXene loadings. Additionally, for comparison, Table S4 in the Supporting Information indicates the maximum dielectric permittivity and corresponding dielectric loss reported in the literature using P(VDF-TrFE-CFE) as the matrix with different conductive fillers.

DOI: 10.1021/acsnano.7b08895
ACS Nano 2018, 12, 3369−3377

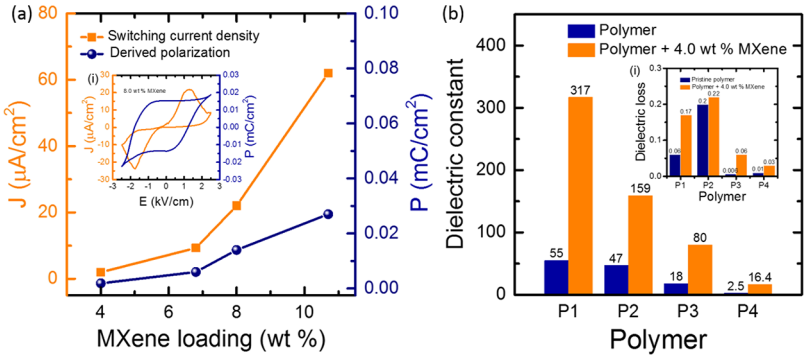

Figure 6. (a) Leakage-corrected switching current density and derived polarization of MXene/P(VDF-TrFE-CFE) composites with different MXene loadings. Inset (i): Leakage-corrected *J*–*E* and *P*–*E* loops of MXene/P(VDF-TrFE-CFE) with 8.0 wt % MXene loading. (b) Dielectric constant of different polymers without and with 4.0 wt % MXene. Inset (i): Dielectric loss of different polymers embedded with 4.0 wt % MXene loading; P1, P(VDF-TrFE-CFE); P2, P(VDF-TrFE-CTFE); P3, P(VDF-TrFE); P4, PVP.

In order to study the mechanism of dielectric constant enhancement observed above, we performed bipolar and unipolar current density *vs* electric field (*J*–*E*) loop measurements on both pristine P(VDF-TrFE-CFE) and MXene/P(VDF-TrFE-CFE) composites.[37] Before either the bipolar or the unipolar loop measurement, the samples were poled negatively by applying an electric field of 2.5 kV cm^{-1} for 5 min at room temperature. Figure 5a illustrates the first and third *J*–*E* curves of the pristine P(VDF-TrFE-CFE) sample measured by applying an electric field from −2.5 to 2.5 kV/cm, which reveals almost no difference between these two curves. This result demonstrates that the pristine terpolymer P(VDF-TrFE-CFE) behaves as a liner dielectric, which is expected given the paraelectric nature of this polymer. Figure 5b displays a sequence of positive unipolar *J*–*E* curves (measured on negatively prepoled terpolymer). As can be seen in Figure 5b, inset (i), the current densities of the P(VDF-TrFE-CFE) sample exhibit no obvious change, even after 19 unipolar cycles. This result is not surprising since the terpolymer is not ferroelectric after 70 °C annealing,[30] so no switching current can be measured. Figure 5b, inset (ii), shows the time-dependent current density of the pristine terpolymer, which was measured by applying a 1.25 kV cm^{-1} electric field and holding it for 1 h. Evidently, the current density quickly decreases before stabilizing at a constant value (9.0×10^{-4} μA/cm^2). The results in Figure 5a and b clearly demonstrate that pristine P(VDF-TrFE-CFE) exhibits a typical paraelectric behavior and no switching current. The XRD analysis (2θ = 16° to 22°) in Figure S3b presents only one sharp peak at 2θ = 18.4°, which indicates that the paraelectric polymer phase is prominent in both the pristine P(VDF-TrFE-CFE) and the MXene/P(VDF-TrFE-CFE) composite.[30]

Figure 5c and d respectively display the bipolar and the unipolar measurement of the MXene/P(VDF-TrFE-CFE) composite. Prior to these measurements, the composite had been poled using negative 2.5 kV cm^{-1} for 5 min at room temperature. Figure 5c shows the first and third *J*–*E* curves measured after negatively poling the sample. These indicate that the introduction of MXene to the terpolymer enables the measurement of a much higher switching current. In Figure 5d, the first unipolar *J*–*E* curve (0 → 2.5 kV cm^{-1}) exhibits a bump at about 1.5 kV cm^{-1}, which must be due to the current induced by some dipole reversal since the sample was previously poled by a negative voltage. In the following *J*–*E* loops (3rd to 19th), no bump was observed in either the increasing-field or decreasing-field curve because most "dipoles" had been aligned in the positive direction during the first positive electric field application.[37] The *J*–*E* curves of MXene/P(VDF-TrFE-CFE) in Figure 5c and d exhibit typical relaxor ferroelectric behavior, which some previous reports have discussed.[38,39] We measured eight samples and found that they all exhibit similar behavior. In addition, the current density decreased and gradually approached a constant value when the field was cycled. In inset (i) of Figure 5d, the current density indicates a clearly decreasing trend as a function of the number of cycles at 2.5 kV cm^{-1}, which could be due to gradually decreasing dipole reversal under the positive unipolar electric field.[40] Relaxation measurements were performed to investigate the relaxation properties of the MXene/P(VDF-TrFE-CFE) composite. Inset (ii) of Figure 5d reveals that the current density experienced an exponential decay, which eq 2 illustrates as follows:

$$\log[J(t)] = a \log(t) + b \tag{2}$$

where $J(t)$ is the current density at time t, and a and b are constants. The substitution of several sets of original data into eq 2 yielded the mean values of constants a (−0.276) and b (−0.1425). Therefore, eq 2 can be written as follows:

$$J(t) = 0.72t^{-0.276} \tag{3}$$

This long relaxation time observed in the MXene/P(VDF-TrFE-CFE) composite (Figure 5d) has significant implications for the mechanism of dielectric constant enhancement, which is discussed shortly.

Figure 6a illustrates the leakage-corrected switching current density (left *y*-axis) and derived polarization (right *y*-axis) of MXene/P(VDF-TrFE-CFE) composites, both of which increase with increasing MXene loadings. The leakage-corrected polarization can be calculated as follows:

$$P(t) = \int_0^t [J(t) - J_d(t)]\, dt \tag{4}$$

where $J(t)$ is the measured total current density, including the current induced by dipole reversal and leakage, and $J_d(t)$ is the measured current density after several cycles of electric field, which approximately represents the leakage current. Inset (i) of Figure 6a depicts the leakage-corrected hysteresis loop and leakage-corrected switching current density of the MXene/P(VDF-TrFE-CFE) composite with 8.0 wt % MXene loading. This result clearly indicates that some switching process takes

DOI: 10.1021/acsnano.7b08895
ACS Nano 2018, 12, 3369–3377

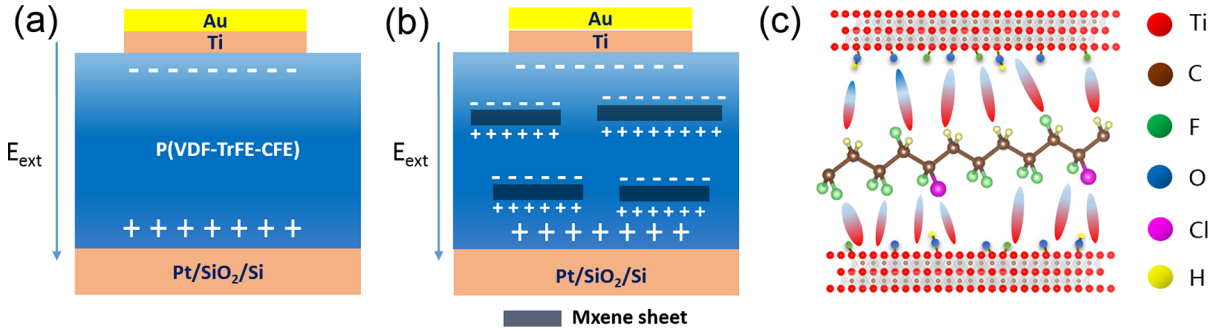

Figure 7. (a, b) Schematic illustration of the polarization charges that exist in pristine P(VDF-TrFE-CFE) and MXene/P(VDF-TrFE-CFE) MIM capacitors under an external electric field (E_{ext}). (c) Schematic illustration of dipoles that may form between MXene surface atoms (F, O) and H on the polymer backbone if polymer chains are intercalated between MXene sheets.

place within the MXene-containing polymer, which is not the case in the pristine P(VDF-TrFE-CFE) polymer. The magnitude of the polarization ranged from 1.9 μC/cm^2 for a sample with 4.0 wt % MXene to 27.0 μC/cm^2 for a sample with 10.7 wt % MXene. These polarization values are relatively large for a polymer and indicate that some other dipole must have formed within the composite that does not exist in the pristine polymer. In fact, we investigated the dielectric constant enhancement of several MXene-loaded insulating polymers (see Figure 6b). These polymers are as follows: P1, poly(vinylidene fluoride-trifluoroethylene-chlorofluoroehylene) (P(VDF-TrFE-CFE)); P2, poly(vinylidene fluoride-trifluoro-ethylene-chlorotrifl uoroethylene) (P(VDF-TrFE-CTFE)); P3, poly(vinylidene fluoride-trifluoroethylene) (P(VDF-TrFE)); and P4, polyvinylpyrrolidone (PVP). With 4.0 wt % MXene loading, the dielectric constants of polymers P1, P2, P3, and P4 increase from 55, 47, 18, and 2.5 to 317, 159, 80, and 16.4, respectively. These results convey that the dielectric constant enhancements in various polymers embedded with MXene are of the same order of magnitude. Inset (i) of Figure 6b reveals that the dielectric loss of several different MXene−polymer composites only slightly increases, while the dielectric constant of the same composites increases significantly after 4.0 wt % MXene loading. Table S5 in the Supporting Information lists a comparison of the dielectric constant and dielectric loss of MXene−polymer composites with 4.0 wt % MXene loading.

Based on the above results, the remaining question is how to explain the significant increase in the dielectric constant of the MXene−polymer composites. Figure 7 displays our proposed mechanism for the origin of the dielectric constant enhancement in the MXene/P(VDF-TrFE-CFE) composite, but the same model applies to all MXene-loaded insulated polymers tested in this study (Figure 6b). Figure 7a presents a schematic illustration of the P(VDF-TrFE-CFE) MIM capacitor, which indicates that the pristine P(VDF-TrFE-CFE) acts as a typical dielectric polymer under an externally applied electric field (E_{ext}). In contrast, the MIM capacitor that uses the MXene/P(VDF-TrFE-CFE) composite as a dielectric layer (Figure 7b) responds differently to the externally applied electric field. Several models have been proposed to explain the dielectric constant enhancement of polymer composites with conductive fillers.[32,41,42] Near percolation, the large increase in the dielectric constant has generally been explained by two main mechanisms, both of which lead to interfacial polarization in the composite bulk at the interfaces between the conducting fillers and the host polymer. These two mechanisms are known as the microcapacitor network model[43] and the microscopic dipole model.[44] In the former, microcapacitors are created when neighboring conductive fillers become so close to each other that they leave only a very thin dielectric layer between them. Because of this thin dielectric layer, each microcapacitor makes a substantial contribution to the capacitance of the microcapacitor network, which results in a much larger dielectric constant near the percolation limit.[32] For conductive spheres in an insulator, a percolation limit of approximately 16 vol % has been predicted, although it can be smaller in practice.[31,45] However, the percolation volume fraction of MXenes in our composite is below 7.0 vol %. In addition, even away from the percolation limit, the dielectric constant of our MXene-based composites could be increased by 1 order of magnitude by merely adding a few percentages of MXene (3.6 vol % or 8 wt %). With such low MXene concentrations, the MXene sheets will be too far apart, which would make it difficult to form microcapacitors with extremely thin polymer layers between the MXene sheets.

Hence, we believe that the microscopic dipole model can more effectively describe the increased dielectric constant of these MXene-containing polymers. In this model, when an electric field (E_{ext}) is applied to the device (Figure 7b), charges accumulate on the interfaces between conductive fillers (MXene sheets in our case) and the polymer matrix, where the microscopic dipoles are situated. This differs from the MXene-free polymer, where the polarization charge is accumulated near the electrodes of the MIM device (Figure 7a). In the microscopic dipole model, the MXene sheets do not need to be as close together as the microcapacitor model requires, which is the case for our samples. The microscopic dipole model can even explain the slow current relaxation that is apparent in Figure 5d, inset (ii). In true metallic fillers embedded in a polymer matrix, the relaxation of charges on the surface of metal fillers should occur rapidly. However, in our MXene/P(VDF-TrFE-CFE) composite, a long relaxation time was observed (see Figure 5d, inset (ii)), which suggests that the positive and negative charges that accumulated on the interfaces between the MXene sheet and the polymer matrix will recombine slowly after the removal of the electric field. We believe that the long relaxation time is due to the fact that the MXene sheets, while metallic, have some polymer chains intercalated between them, as indicated by the increased interlayer spacing of MXene (from 1.2 to 1.4 nm) (see Figure 3d, Table S1, and Figure S3a). These polymer chains can slow down the recombination of the accumulated charges (at the interfaces between the MXene sheets and the polymer) after the removal of the external electric field.

DOI: 10.1021/acsnano.7b08895
ACS Nano 2018, 12, 3369−3377

Finally, these MXenes−polymer composites may feature a special type of polarization deriving from hydrogen bonds that can form at any point where polymer chains manage to intercalate between the MXene sheets (see Figure 7c). As mentioned earlier, XRD data in Figure 3d, Table S1, and Figure S3 indicate that the MXene interlayer spacing expands at a higher polymer content, which suggests that some polymer chains may have successfully intercalated between MXene sheets. The hydrogen bonds between negative charges on the MXene surface (*e.g.*, F and O) and H atoms on the polymer backbone can form a dipole that responds to the applied electric field. A previous report[46] has proposed the large dipole moment of such hydrogen bonds as the key factor for dielectric constant enhancement of a PVDF/hydrated metal salt composite. Moreover, another study has calculated the dielectric constant enhancement factor due to hydrogen bonds to be approximately 3 through a comparison of the dielectric constant of hydrogen-bonded and dipolar aprotic solvents.[47] Since the H−F and H−O bonds can exist in MXene−polymer composites, we surmise that hydrogen bonding between the atoms on the MXene surface and an H atom on the polymer backbone could contribute to the enhanced dielectric constant in our composites.

CONCLUSION

We have demonstrated that dispersing MXene in the P(VDF-TrFE-CFE) matrix induces a large enhancement of the dielectric constant, which can reach as high as 10^5 near the percolation limit of 15.3 wt % MXene loading. The ratio of the dielectric constant to loss tangent for MXene-loaded composites outperforms all previously reported conductive fillers incorporated in the same polymer. Current voltage and current relaxation measurements suggest that the origin of the substantial permittivity enhancement is primarily due to the microscopic dipoles formed by the accumulation of charges at the interfaces between the MXene fillers and the polymer matrix. This dielectric constant enhancement by MXene dispersion is also observed in other insulating polymers.

METHODS

Preparation of MXene. All chemicals were used as received without further purification. Layered ternary carbide Ti_3AlC_2 (MAX phase) powder was commercially procured (Carbon-Ukraine Ltd., particle size <40 μm). $Ti_3C_2T_x$ MXene was synthesized following the minimally intensive layer delamination (MILD) method, which entailed selective etching of aluminum from Ti_3AlC_2 using *in situ* HF-forming etchant as previously reported in extensive detail.[48] The etching solution was prepared by adding 1 g of lithium fluoride (LiF, Alfa Aesar, 98+%) to 20 mL of 9 M hydrochloric acid (HCl, Fisher, technical grade, 35−38%) followed by stirring for 5 min. Then, 1 g of Ti_3AlC_2 powder was slowly added to the MILD etchant at 35 °C and stirred for 24 h. The acidic suspension was washed with deionized water until pH > 6 *via* centrifugation at 3500 rpm (5 min per cycle), with decanting of the supernatant after each cycle. Around pH ≥ 6, a stable dark green supernatant of $Ti_3C_2T_x$ was observed and then collected after 5 min of centrifugation at 3500 rpm. The concentration of the $Ti_3C_2T_x$ solution was measured by filtering specific amounts of colloidal solution through a polypropylene filter (3501 coated PP, Celgard LLC, Charlotte, NC, USA), followed by overnight drying under a vacuum at 70 °C. The electrical conductivity (5500 S/m) of $Ti_3C_2T_x$ MXene sheets was was determined with a Keithley four-point probe meter.

Fabrication of Nanocomposites. MXene sheets were weighed according to the desired filler loadings, suspended in 3 mL of dimethylformamide, and dispersed *via* shaking for 1 h. Subsequently, 300 mg of P(VDF-TrFE-CFE) (61.5/30.2/8.3 mol % Piezotech S.A., France), P(VDF-TrFE-CTFE) (66.5/24.9/8.6 mol % Piezotech S.A., France), P(VDF-TrFE) (70/30 mol % Piezotech S.A., France), and PVP (Sigma-Aldrich, USA) were dissolved into the suspensions under continuous stirring for 30 min at 80 °C. The MXene−polymer solutions were then ultrasonicated for 2 h, and the dispersion was cast directly onto platinum-coated silicon substrates. The samples were then dried overnight in an oxygen-free glovebox and were finally annealed at 70 °C in a vacuum oven for 2 days. For dielectric characterization, top Ti (100 nm)/Au (50 nm) electrodes were deposited on the films (with an average thickness of 100 μm) by electron-beam evaporation through a shadow mask.

Equipment and Characterization. Thermogravimetric analysis confirmed the weight percent of MXene in the matrix. In addition, the structure and properties of MXene−polymer composites were studied using XRD (Bruker D2 Phaser) and FT-IR in transmission mode (Nicolet iS10, Thermo Scientific). Raman spectroscopy was performed on a Horiba Aramis Raman microscope with 633 nm laser excitation. The MXene sheets were investigated with TEM (Titan Cs Image), SEM (Nova Nano), and XPS (Amicus). The electrical conductivity of the MXene sheets was investigated with a Keithley four-point probe meter (model: 195 A, detection limit: 20 MΩ). Surface and cross-sectional images of composite films were observed with TEM (Titan Cs Image). Frequency-dependent capacitance was measured with an Agilent LCR meter (4980A) in the frequency range of 1K Hz to 100 kHz and an oscillation signal of ~50 mV_{rms} with a parallel equivalent circuit. The current density *vs* electric field ($J-E$) loops in our article were derived from $I-V$ curves measured by an Agilent B1500A system. The $J-E$ loops were measured by using a direct current source with a field ramping rate of 50 V cm^{-1} s^{-1}. The dwell time was 0.5 s for each step.

ASSOCIATED CONTENT

Supporting Information

The Supporting Information is available free of charge on the ACS Publications website at DOI: 10.1021/acsnano.7b08895.

Figures: Thermogravimetric analysis of MXene/P(VDF-TrFE-CFE) composites; X-ray photoelectron spectroscopy spectra of $Ti_3C_2T_x$, Ti 2p, C 1s; X-ray diffraction characteristic peak of MXene/P(VDF-TrFE-CFE) composites; dielectric constant, dielectric loss, and conductivity of MXene/P(VDF-TrFE-CFE) composites with different MXene loadings; Tables: Diffraction peak angle and interlayer spacing of MXene in P(VDF-TrFE-CFE) matrix with different polymer loading; weight percent and volume fration of MXene sheets embedded in P(VDF-TrFE-CFE) matrix; dielectric permittivity and dielectric loss of MXene/P(VDF-TrFE-CFE) with different MXene loadings; maximum dielectric permittivity and corresponding dielectric loss reported in the literature using P(VDF-TrFE-CFE) as matrix with different conductive fillers; dielectric constant enhancement factor of MXene/polymer composites with MXene embedded in different polymer matrices (PDF)

AUTHOR INFORMATION

Corresponding Authors

*E-mail: xixiang.zhang@kaust.edu.sa.
*E-mail: husam.alshareef@kaust.edu.sa.

ORCID

Shaobo Tu: 0000-0002-9684-689X
Xixiang Zhang: 0000-0002-3478-6414
Husam N. Alshareef: 0000-0001-5029-2142

Author Contributions

†S. Tu and Q. Jiang contributed equally to the work.

DOI: 10.1021/acsnano.7b08895
ACS Nano 2018, 12, 3369−3377

Notes

The authors declare no competing financial interest.

ACKNOWLEDGMENTS

Research reported in this publication is supported by King Abdullah University of Science and Technology (KAUST). The authors would like to thank the Advanced Nanofabrication, Imaging and Characterization Laboratory at KAUST for their excellent assistance.

REFERENCES

(1) Dang, Z. M.; Wang, L.; Yin, Y.; Zhang, Q.; Lei, Q. Q. Giant Dielectric Permittivities in Functionalized Carbon-Nanotube/ Electroactive-Polymer Nanocomposites. *Adv. Mater.* **2007**, *19*, 852−857.

(2) Dang, Z. M.; Wang, L.; Wang, H. Y.; Nan, C. W.; Xie, D.; Yin, Y.; Tjong, S. C. Rescaled Temperature Dependence of Dielectric Behavior of Ferroelectric Polymer Composites. *Appl. Phys. Lett.* **2005**, *86*, 172905.

(3) Lee, Y. T.; Kwon, H.; Kim, J. S.; Kim, H. H.; Lee, Y. J.; Lim, J. A.; Song, Y. W.; Yi, Y. J.; Choi, W. K.; Hwang, D. K.; Im, S. Noncolatile Ferroelectric Memory Circuit Using Black Phosphorus Nanosheet-Based Field-Effect Transistors with P(VDF-TrFE) Polymer. *ACS Nano* **2015**, *9*, 10394−10401.

(4) Elshurafa, A. M.; Almadhoun, M. N.; Salama, K. N.; Alshareef, H. N. Microscale Electrostatic Fractional Capacitors Using Reduced Graphene Oxide Percolated Polymer Composites. *Appl. Phys. Lett.* **2013**, *102*, 232901.

(5) Yang, Y.; Zhang, H. L.; Zhu, G.; Lee, S. M.; Lin, Z. H.; Wang, Z. L. Flexible Hybrid Energy Cell for Simultaneously Haverting Thermal, Mechanical, and Solar Energies. *ACS Nano* **2013**, *7*, 785−790.

(6) Zhang, B.; Zhang, L.; Deng, W.; Jin, L.; Chun, F.; Pan, H.; Gu, B.; Zhang, H.; Lv, Z.; Yang, W.; Wang, Z. L. Self-Powered Acceleratin Sensor Based on Liquid Metal Triboelectric Nanogenerator for Vibration Monitoring. *ACS Nano* **2017**, *11*, 7440−7446.

(7) Dang, Z. M.; Wu, J. P.; Xu, H. P.; Yao, S. H.; Jiang, M. J.; Bai, J. Dielectric Properties of Upright Carbon Fiber Filled Poly(vinylidene fluoride) Composite with Low Percolation Threshold and Weak Temperature Dependence. *Appl. Phys. Lett.* **2007**, *91*, 072912.

(8) Fan, P.; Wang, L.; Yang, J.; Chen, F.; Zhong, M. Graphene/ Poly(vinylidene fluoride) Composites with High Dielectric Constant and Low Percolation Threshold. *Nanotechnology* **2012**, *23*, 365702.

(9) Garrett, J. T.; Roland, C. M.; Petchsuk, A.; Chung, T. C. Electrostrictive Behavior of Poly(vinylidene fluoride-trifluoroethylene-chlorotrifluoroethylene). *Appl. Phys. Lett.* **2003**, *83*, 1190−1192.

(10) Han, K.; Li, Q.; Chen, Z.; Gadinski, M. R.; Dong, L.; Xiong, C.; Wang, Q. Suppression of Energy Dissipation and Enhancement of Breakdown Strength in Ferroelectric Polymer−Graphene Percolative Composites. *J. Mater. Chem. C* **2013**, *1*, 7034−7042.

(11) Han, Z.; Li, D.; Wang, X. W.; Zhang, Z. D. Microwave Response of FeCo/Carbon Nanotubes Composites. *J. Appl. Phys.* **2011**, *109*, 07A301.

(12) Almadhoun, M. N.; Hedhili, M. N.; Odeh, I. N.; Xavier, P.; Bhansali, U. S.; Alshareef, H. N. Influence of Stacking Morphology and Edge Nitrogen Doping on the Dielectric Performance of Graphene−Polymer Nanocomposites. *Chem. Mater.* **2014**, *26*, 2856−2861.

(13) Zhang, S. H.; Zhang, N. Y.; Huang, C.; Ren, K. L.; Zhang, Q. M. Microstructure and Electromechanical Properties of Carbon Nanotube/Poly(vinylidene fluoride-trefluoroethylene-chlorofluoroethylene) Composites. *Adv. Mater.* **2005**, *17*, 1897−1901.

(14) Wang, J. W.; Shen, Q. D.; Bao, H. M.; Yang, C. Z. Microstructure and Dielectric Properties of P(VDF-TrFE-CFE) with Partially Grafted Copper Phthalocyanine Oligomer. *Macromolecules* **2007**, *38*, 2247−2252.

(15) Huang, C.; Zhang, Q. M. Enhanced Dielectric and Electromechanical Responses in High Dielectric Constant All-Polymer Percolative Composites. *Adv. Funct. Mater.* **2004**, *14*, 501−506.

(16) Javadi, A.; Xiao, Y.; Xu, W.; Gong, S. Chemically Modified Graphene/P(VDF-TrFE-CFE) Electroactive Polymer Nanocomposites with Superior Electromechanical Performance. *J. Mater. Chem.* **2012**, *22*, 830−834.

(17) Naguib, M.; Kurtoglu, M.; Presser, V.; Lu, J.; Niu, J.; Heon, M.; Hultman, L.; Gogotsi, Y.; Barsoum, M. W. Two-Dimensional Nanocrystals Produced by Exfoliation of Ti_3AlC_2. *Adv. Mater.* **2011**, *23*, 4248−4253.

(18) Hope, M. A.; Forse, A. C.; Griffith, K. J.; Lukatskaya, M. R.; Ghidiu, M.; Gogotsi, Y.; Grey, C. P. NMR Reveals the Surface Functionalisation of Ti_3C_2 MXene. *Phys. Chem. Chem. Phys.* **2016**, *18*, 5099−5102.

(19) Römer, F. M.; Wiedwald, U.; Strusch, T.; Halim, J.; Mayerberger, E.; Barsoum, M. W.; Farle, M. Controlling the Conductivity of Ti_3C_2 MXenes by Inductively Coupled Oxygen and Hydrogen Plasma Treatment and Humidity. *RSC Adv.* **2017**, *7*, 13097−13103.

(20) Anasori, B.; Lukatskaya, M. R.; Gogotsi, Y. 2D Metal Carbides and Nitrides (MXenes) for Energy Storage. *Nat. Rev. Mater.* **2017**, *2*, 16098.

(21) Kim, H.; Anasori, B.; Gogotsi, Y.; Alshareef, H. N. Thermoelectric Properties of Two-Dimensional Molybdenum-Based MXenes. *Chem. Mater.* **2017**, *29*, 6472−6479.

(22) Jiang, Q.; Wu, C.; Wang, Z.; Wang, A. C.; He, J. H.; Wang, Z. L.; Alshareef, H. N. MXene Electrochemical Microsupercapacitor Integrated with Triboelectric Nanogenerator as a Wearable Self-Charging Power Unit. *Nano Energy* **2018**, *45*, 266−272.

(23) Xu, B.; Zhu, M.; Zhang, W.; Zhen, X.; Pei, Z.; Xue, Q.; Zhi, C.; Shi, P. Ultrathin MXene-Micropattern-Based Field-Effect Transistor for Probing Neural Activity. *Adv. Mater.* **2016**, *28*, 3333−3339.

(24) Naguib, M.; Mashtalir, O.; Carle, J.; Presser, V.; Lu, J.; Hultman, L.; Gogotsi, Y.; Barsoum, M. W. Two-Dimensional Transition Metal Carbides. *ACS Nano* **2012**, *6*, 1322−1331.

(25) Hu, T.; Wang, J.; Zhang, H.; Li, Z.; Hu, M.; Wang, X. Vibrational Properties of Ti_3C_2 and $Ti_3C_2T_2$ (T = O, F, OH) Monosheets by First-principles Calculations: A Comparative Study. *Phys. Chem. Chem. Phys.* **2015**, *17*, 9997−10003.

(26) Lisowski, W.; Berg, A. H. J.; Leonard, D.; Mathieu, H. J. Characterization of Titanium Hydride Films Covered by Nanoscale Evaporated Au Layers: ToF-SIMS, XPS and AES Depth Profile Analysis. Surf. *Surf. Interface Anal.* **2000**, *29*, 292−297.

(27) Halim, J.; Cook, K. M.; Naguib, M.; Eklund, P.; Gogotsi, Y.; Rosen, J.; Barsoum, M. W. X-ray Photoelectron Spectroscopy of Select Multi-Layered Transition Metal Carbides (MXenes). *Appl. Surf. Sci.* **2016**, *362*, 406−417.

(28) Zhu, M.; Huang, Y.; Deng, Q.; Zhou, J.; Pei, Z.; Xue, Q.; Huang, Y.; Wang, Z.; Li, H.; Huang, Q.; Zhi, C. Highly Flexible, Freestanding Supercapacitor Electrode with Enhanced Performance Obtained by Hybridizing Polypyrrole Chains with MXene. *Adv. Energy Mater.* **2016**, *6*, 1600969.

(29) Kobayashi, M.; Tashiro, K.; Tadokoro, H. Molecular Vibrations of Three Crystal Forms of Poly(vinylidene fluoride). *Macromolecules* **1975**, *8*, 158−171.

(30) Bao, H. M.; Song, J. F.; Zhang, J.; Shen, Q. D.; Yang, C. Z. Phase Transitions and Ferroelectric Relaxor Behavior in P(VDf-TrFE-CFE) Terpolymers. *Macromolecules* **2007**, *40*, 2371−2379.

(31) Nan, C. W.; Shen, Y.; Ma, J. Physical Properties of Composites Near Percolation. *Annu. Rev. Mater. Res.* **2010**, *40*, 131−151.

(32) Zhang, L.; Shan, X.; Bass, P.; Tong, Y.; Rolin, T. D.; Hill, C. W.; Brewer, J. C.; Tucker, D. S.; Cheng, Z. Y. Process and Microstructure to Achieve Ultra-high Dielectric Constant in Ceramic-Polymer Composites. *Sci. Rep.* **2016**, *6*, 35763.

(33) Nan, C. W. Physics of Inhomogeneous Inorganic Materials. *Prog. Mater. Sci.* **1993**, *37*, 1−116.

(34) Rahaman, M.; Chaki, T. K.; Khastgir, D. Modeling of DC conductivity for Ethylene Vinyl Acetate (EVA)/Polyaniline Conductive Composites Prepared Through Insitu Polymerization of Aniline in EVA Matrix. *Compos. Sci. Technol.* **2012**, *72*, 1575−1580.

(35) Dang, Z.-M.; Nan, C.-W.; Xie, D.; Zhang, Y.-H.; Tjong, S. C. Dielectric Behavior and Dependence of Percolation Threshold on The

DOI: 10.1021/acsnano.7b08895
ACS Nano 2018, 12, 3369−3377

Conductivity of Fillers in Polymer-Semiconductor Composites. *Appl. Phys. Lett.* **2004**, *85*, 97−99.
(36) Nan, C. W.; Shen, Y.; Ma, J. Physical Properties of Composites Near Percolation. *Annu. Rev. Mater. Res.* **2010**, *40*, 131−151.
(37) Dickens, B.; Balizer, E.; DeReggi, A. S.; Roth, S. C. Hysteresis Measurements of Remanent Polarization and Coercive Field in Polymers. *J. Appl. Phys.* **1992**, *72*, 4258−4264.
(38) Zhu, L. Exploring Strategies for High Dielectric Constant and Low Loss Polymer Dielectrics. *J. Phys. Chem. Lett.* **2014**, *5*, 3677−3687.
(39) Prateek; Thakur, V. K.; Gupta, R. K. Recent Progress on Ferroelectric Polymer-Based Nanocomposites for High Energy Density Capacitors: Synthesis, Dielectric Properties, and Future Aspects. *Chem. Rev.* **2016**, *116*, 4260−4317.
(40) Yao, Y.; Wang, Q.; Wang, H.; Zhang, B.; Zhao, C.; Wang, Z.; Xu, Z.; Wu, Y.; Huang, W.; Qian, P. Y.; Zhang, X. X. Bio-Assembled Nanocomposites in Conch Shells Exhibit Giant Electret Hysteresis. *Adv. Mater.* **2013**, *25*, 711−718.
(41) Simpkin, R. Derivation of Lichtenecker's Logarithmic Mixture Formula From Maxwell's Equations. *IEEE Trans. Microwave Theory Tech.* **2010**, *58*, 545−550.
(42) Wilkinson, D.; Langer, J. S.; Sen, P. N. Enhancement of The Dielectric Constant Near A Percolation Threshold. *Phys. Rev. B: Condens. Matter Mater. Phys.* **1983**, *28*, 1081−1087.
(43) Lei, T.; Xue, Q.; Chu, L.; Han, Z.; Sun, J.; Xia, F.; Zhang, Z.; Guo, Q. Excellent Dielectric Properties of Polymer Composites Based on Core-Shell Structured Carbon/Silica Nanohybrid. *Appl. Phys. Lett.* **2013**, *103*, 012902.
(44) Bauer, S.; Gerhard-Multhaupt, R.; Sessler, G. M. Ferroelectrets: Soft Electroactive Foams for Transducers. Phys. *Phys. Today* **2004**, *57*, 37−43.
(45) Dang, Z. M.; Yuan, J. K.; Yao, S. H.; Liao, R. J. Flexible Nanodielectric Materials with High Permittivity for Power Energy Storage. *Adv. Mater.* **2013**, *25*, 6334−6365.
(46) Jana, S.; Garain, S.; Sen, S.; Mandal, D. The Influence of Hydrogen Bonding on The Dielectric Constant and The Piezoelectric Energy Harvesting Performance of Hydrated Metal Salt Mediated PVDF Films. *Phys. Chem. Chem. Phys.* **2015**, *17*, 17429−17436.
(47) Goldman, S.; Joslin, C. Why Hydrogen-Bonded Liquids Tend to Have High Static Dielectric Constants. *J. Phys. Chem.* **1993**, *97*, 12349−12355.
(48) Zhang, C. J.; Pinilla, S.; McEvoy, N.; Cullen, C. P.; Anasori, B.; Long, E.; Park, S.-H.; Seral-Ascaso, A.; Shmeliov, A.; Krishnan, D.; Morant, C.; Liu, X.; Duesberg, G. S.; Gogotsi, Y.; Nicolosi, V. Oxidation Stability of Colloidal Two-Dimensional Titanium Carbides (MXenes). *Chem. Mater.* **2017**, *29*, 4848−4856.

DOI: 10.1021/acsnano.7b08895
ACS Nano 2018, 12, 3369−3377